Supplementary Data

Insights into the Mechanism of Cystatin C Oligomer and Amyloid Formation and its Interaction with Beta-Amyloid

Tyler J. Perlenfein, Jacob D. Mehlhoff, Regina M. Murphy

This section contains the following supplementary data and information:

- Expansion on the analysis of DLS and SLS data
- Supplementary Figure S1: CD spectra of mCys, dCys, and oCys
- Supplementary Figure S2: Molecular structure of dCys with particular attention to arrangement of W106 on adjacent strands
- Supplementary Figure S3: W106 homoFRET detection by 310/295 anisotropy ratio

  Supplementary Figure S4: W106 fluorescence emission spectra of native mCys, dCys, and oCys
- Supplementary Figure S5: Expanded dot blot data set, including total protein control

Analysis of DLS. The diffusive motion of particles in solution give rise to fluctuations in the intensity of scattered light. In DLS, fluctuations are detected and analyzed to generate a normalized first-order autocorrelation function $g^{(1)}(\tau)$. For a dilute solution of monodisperse particles that are small relative to the wavelength of the incident beam (<~λ/20, or ~20 nm),

$$g^{(1)}(\tau) = exp(-Dq^2\tau)$$

where q is the scattering vector and D is the translational diffusion coefficient. D is related to the hydrodynamic diameter d_h of the particle by the Stokes-Einstein equation:

$$d_h = kT/3\pi\eta D$$

where k is the Boltzman constant, T is temperature, and η is solution viscosity. For polydisperse mixtures, $g^{(1)}(\tau)$ is a sum of contributions from all particles. The method of cumulants is used to extract a z-average diffusion coefficient $\langle D \rangle_z$ and a measure of polydispersity μ_2 by fitting the autocorrelation data to

$$\ln g^{(1)}(\tau) = -\langle D \rangle_z q^2\tau + \frac{\mu_2}{2}\tau^2$$

where

$$\langle D \rangle_z = \frac{\sum c_i M_i D_i}{\sum c_i M_i}$$

and c_i, M_i and D_i are the mass concentration, molar mass, and translational diffusion coefficient, respectively, of particles of size i, and the summation is taken over all i particles. The z-average (or, more precisely, the inverse z-averaged) hydrodynamic diameter is then calculated using the Stokes-Einstein equation.

More sophisticated methods of data analysis of polydisperse solutions are available, of which CONTIN (constrained regularization) is one of the most widely used. Briefly, CONTIN finds the intensity-weighted distribution of particle sizes $G(D)$ that best fits the autocorrelation function, with a bias towards smooth distributions:

$$g^{(1)}(\tau) = \int_0^\infty G(D)\, exp(-Dq^2\tau) dD$$

Analysis of SLS. In SLS, the average intensity of scattered light from the sample $I_s(q)$ is measured as a function of the scattering vector (scattering angle) q. Scattering from the buffer is subtracted, and the data are normalized to a reference to account for instrument performance, yielding the Rayleigh ratio $R_s(q)$. For dilute solutions of particles small relative to the wavelength of the incident beam, the weight-averaged molecular weight $\langle M \rangle_w$ is obtained by fitting the angular-dependent scattering:

$$\langle M \rangle_w = \frac{R_s(q)}{Kc}$$

where K is a function of the solution refractive index and the solute refractive index increment, c is the mass concentration, and

$$\langle M \rangle_w = \frac{\sum c_i M_i}{\sum c_i}$$

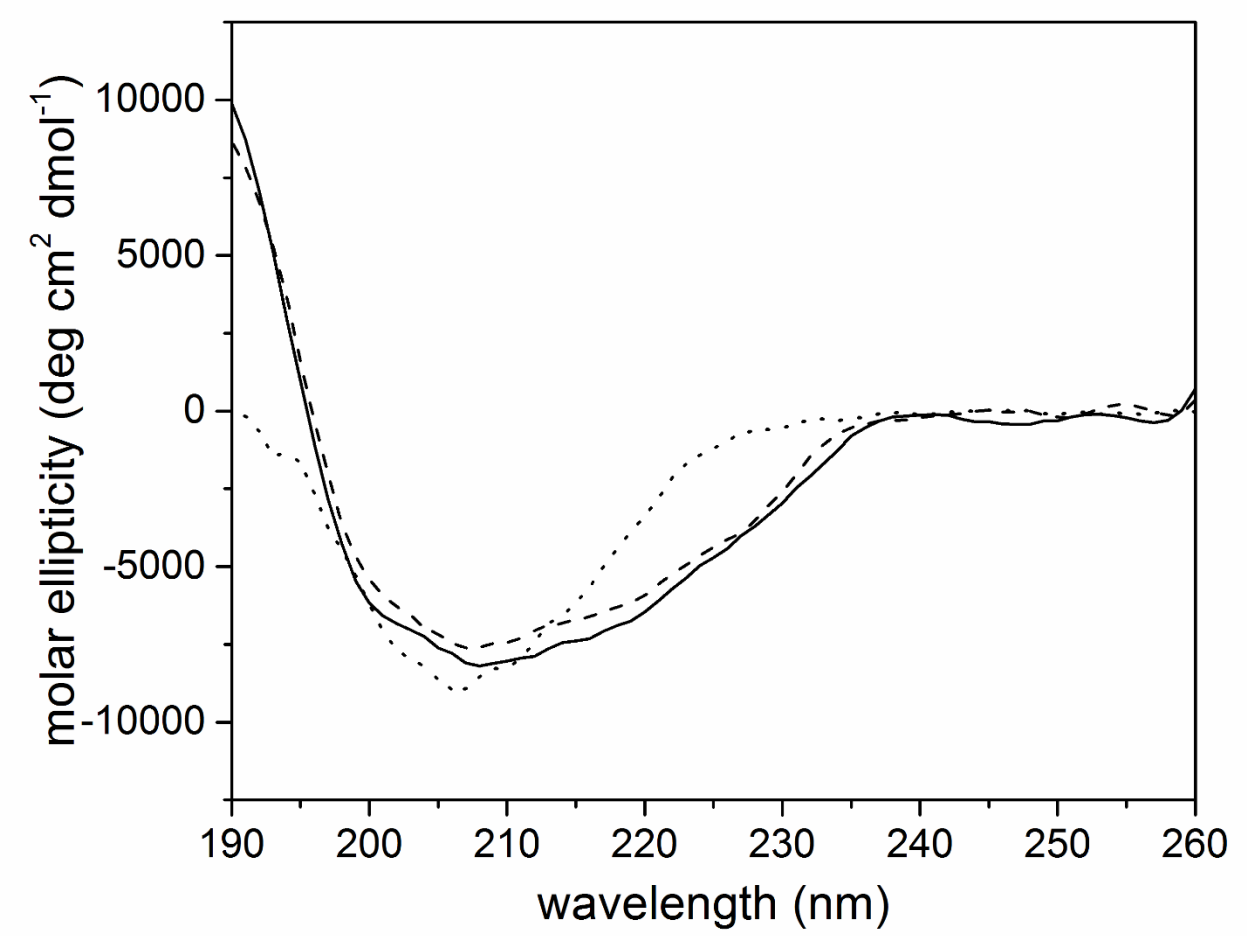

Supplementary Figure S1. CD spectra of mCys (solid line), oCys (dashed line), and dCys (dotted line). Protein samples (20 μM in PBSA-E) were dialyzed extensively into 10 mM phosphate, 50 mM NaF, pH 7.4. Measurements of CD spectra were made on an Aviv model 420 and buffer background was subtracted. Spectral deconvolution was performed using the CDPro package (1). Data shown is the average of 3 scans.

Supplementary Figure S2. Structure of domain-swapped CysC with W106 residues highlighted (PDB: 1R4C). The Förster radius for Trp homoFRET is between 6-16 Å (2, 3), thus the ~13 Å distance between W106 residues on adjacent strands of dCys could be sufficient for FRET. Examples of Trp homoFRET can be seen in apoflavodoxin (3), monoclonal antibodies (4), and as a structural probe for self-assembling peptides (5).

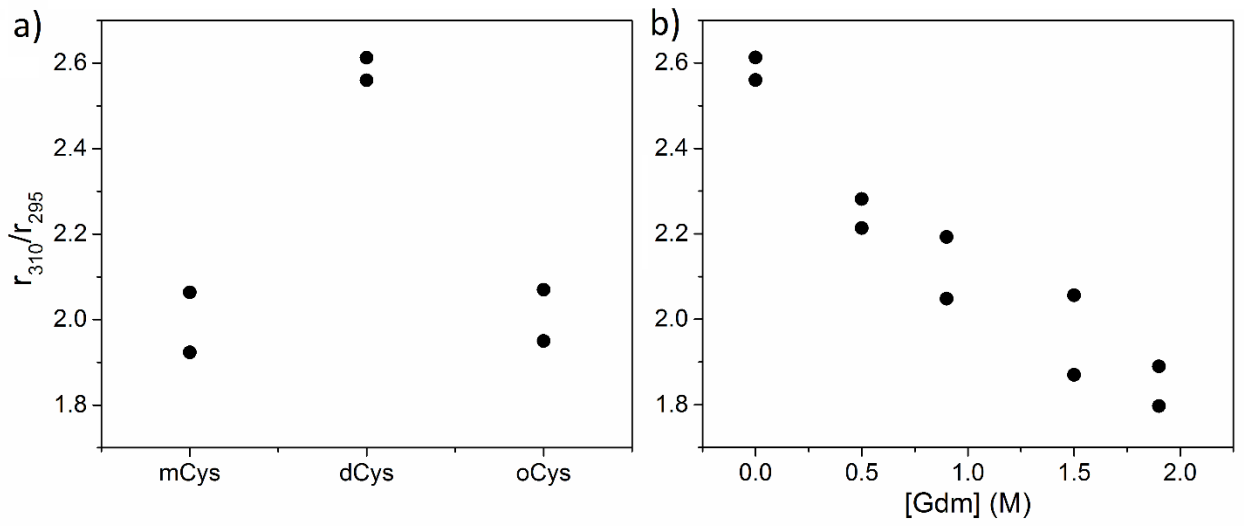

Supplementary Figure S3. W106 homoFRET characterization by anisotropy ratio. Trp homoFRET efficiency is drastically reduced during red-edge excitation compared to excitation at the absorption maxima (6). The ratio of Trp anisotropy at 310 and 295 nm excitation can be used to detect homoFRET activity (7). mCys, dCys, and oCys (9 μM in PBSA-E) were excited at either 295 nm or 310 nm on a QuantaMaster 40 fluorometer with excitation and emission polarization filters (PTI). Parallel and perpendicular emission intensities at 350 nm were measured. The g-factor was measured and anisotropy was calculated as described previously (8, 9). (a) Anisotropy ratios for each CysC preparation in physiological buffer were calculated. The large anisotropy ratio of dCys compared to mCys or oCys indicates homoFRET is likely occurring in dCys, but not mCys or oCys (7). (b) W106 homoFRET is expected to decrease upon dimer dissociation. The anisotropy ratio of dCys was monitored as a function of Gdm concentration. Two independent samples are shown for each experiment.

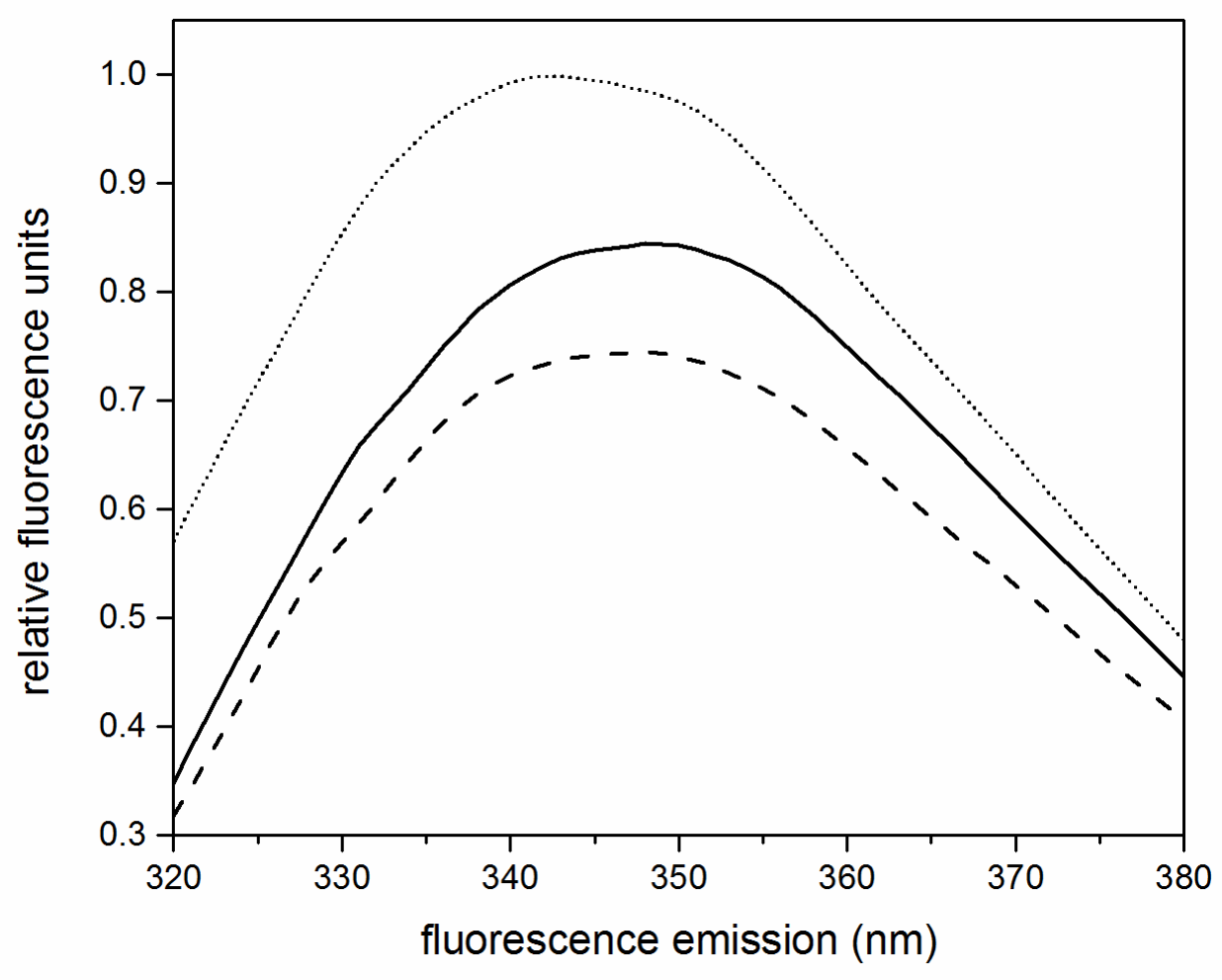

Supplementary Figure S4. Native W106 fluorescence of mCys (solid line), oCys (dashed line), and dCys (dotted line). Protein samples at 9 μM in PBSA-E were excited at 295 nm. Data shown is the average of 3 scans.

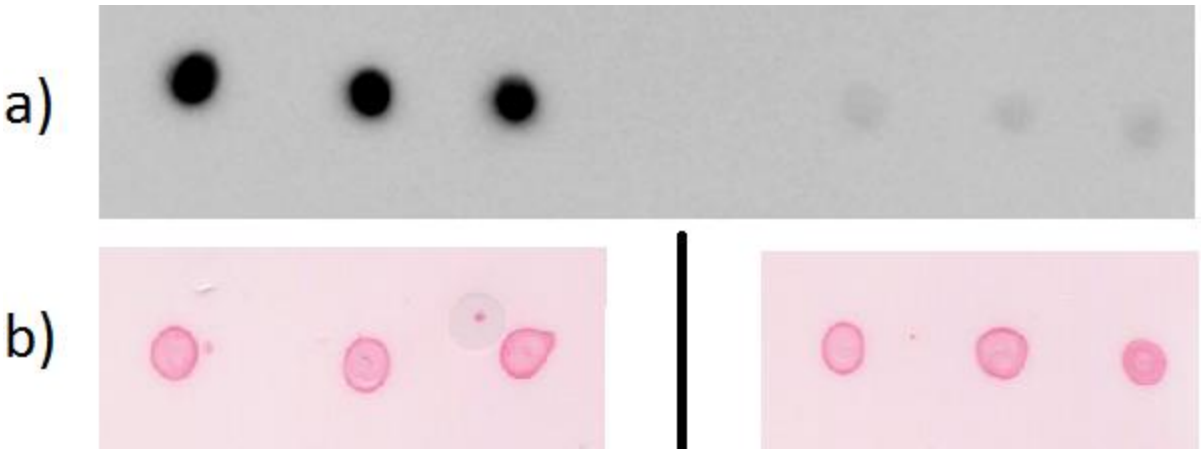

Supplementary Figure S5. Replicates of mCys vs. oCys dot blot experiment comparing C-27 antibody binding. (a) Equal mass of mCys (left) and oCys (right) were spotted onto a nitrocellulose membrane and probed using C-27 (N-terminal) antibody. (b) On a separate membrane, equal mass of mCys (left) and oCys (right) were spotted and probed using Ponceau S (Sigma), a dye which nonspecifically binds proteins and thus can be used to visualize total protein loading (10).

References

1. Sreerama, N., and Woody, R. W. (2000) Estimation of protein secondary structure from circular dichroism spectra: comparison of CONTIN, SELCON, and CDSSTR methods with an expanded reference set. *Anal. Biochem.* **287**, 252–260

2. Karreman, G., Steele, R. H., and Szent-Gyorgyi, A. (1958) On Resonance Transfer of Excitation Energy Between Aromatic Aminoacids in Proteins. *Proc. Natl. Acad. Sci. U. S. A.* **44**, 140–143

3. Visser, N. V, Westphal, A. H., van Hoek, A., van Mierlo, C. P., Visser, A. J., and van Amerongen, H. (2008) Tryptophan-tryptophan energy migration as a tool to follow apoflavodoxin folding. *Biophys J.* **95**, 2462–2469

4. Kayser, V., Chennamsetty, N., Voynov, V., Helk, B., and Trout, B. L. (2011) Tryptophan-Tryptophan Energy Transfer and Classification of Tryptophan Residues in Proteins Using a Therapeutic Monoclonal Antibody as a Model. *J. Fluoresc.* **21**, 275–288

5. Kayser, V., Turton, D. a, Aggeli, A., Beevers, A., Reid, G. D., and Beddard, G. S. (2004) Energy migration in novel pH-triggered self-assembled beta-sheet ribbons. *J. Am. Chem. Soc.* **126**, 336–343

6. Weber, G., and Shinitzky, M. (1970) Failure of energy transfer between identical aromatic molecules on excitation at the long wave edge of the absorption spectrum. *Proc. Natl. Acad. Sci.* **65**, 823–830

7. Moens, P. D. J., Helms, M. K., and Jameson, D. M. (2004) Detection of tryptophan to tryptophan energy transfer in proteins. *Protein J.* **23**, 79–83

8. Kremer, J.J.; Pallitto, M.M.; Sklansky, D.J.; Murphy, R. M. (2000) Correlation of -Amyloid Aggregate Size and Hydrophobicity with Decreased Bilayer Fluidity of Model Membranes. *Biochemistry*. **39**, 10309–10318

9. Lakowicz, J. R. (2006) *Principles of Fluorescence Spectroscopy*, 3rd Ed., Springer, 10.1007/978-0-387-46312-4

10. Romero-Calvo, I., Ocón, B., Martínez-Moya, P., Suárez, M. D., Zarzuelo, A., Martínez-Augustin, O., and de Medina, F. S. (2010) Reversible Ponceau staining as a loading control alternative to actin in Western blots. *Anal. Biochem.* **401**, 318–320